



Cooling radiative forcing effect enhancement of atmospheric amines and mineral particles caused by heterogeneous uptake and oxidation

Weina Zhang^{1,2}, Jianhua Mai¹, Zhichao Fan¹, Yongpeng Ji¹, Yuemeng Ji^{1,2}, Guiying Li^{1,2}, Yanpeng Gao^{1,2}, and Taicheng An^{1,2}

¹Guangdong-Hong Kong-Macao Joint Laboratory for Contaminants Exposure and Health, Guangdong Key Laboratory of Environmental Catalysis and Health Risk Control, Institute of Environmental Health and Pollution Control, Guangdong University of Technology, Guangzhou, 510006, China

²Guangzhou Key Laboratory of Environmental Catalysis and Pollution Control, Key Laboratory of City Cluster Environmental Safety and Green Development of Ministry of Education, School of Environmental Science and Engineering, Guangdong University of Technology, Guangzhou, 510006, China

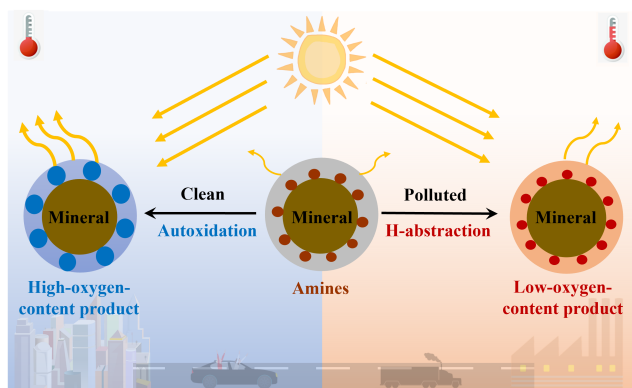
Correspondence: Taicheng An (antc99@gdut.edu.cn)

Received: 6 April 2024 – Discussion started: 22 April 2024

Revised: 8 June 2024 – Accepted: 26 June 2024 – Published: 19 August 2024

Abstract. The warming radiative forcing effect (RFE) derived from atmospheric amines attracts a lot of attention because of their contribution to brown carbon. Herein, the enhanced influence of amines (methyl-, dimethyl-, and trimethylamine) on cooling RFE of mineral particles is first confirmed at visible wavelengths. Present results state heterogeneous uptake and oxidation reactions of atmospheric amines are feasible on mineral particles under clean and polluted conditions, which are proven by related thermodynamics and kinetics data obtained using combined classical molecular dynamics and density function theory methods. Based on mineral particles, simple forcing efficiency (SFE) results explain that amine uptake induces at least 11.8 %–29.5 % enhancement on cooling RFE of amine–mineral particles at visible wavelengths. After amine heterogeneous oxidation, oxidized amine–mineral particle cooling RFEs are furthermore enhanced due to increased oxygen contents. Moreover, oxidized amine–mineral particles under clean conditions show 27.1 %–47.1 % SFE increments at 400–600 nm, which is at least 11.3 % higher than that of itself under polluted conditions, due to high-oxygen-content product formation through amine autoxidation. Our results suggest cooling RFE derived from atmospheric amines can be equally important to their warming RFE on the atmosphere. It is necessary to update the heterogeneous oxidation mechanism and kinetics data of amines in atmospheric models in order to accurately evaluate the whole RFE caused by amines on the atmosphere.

Graphical abstract



1 Introduction

Amines are frequently found in organic aerosols and contribute 11.0 % of $PM_{2.5}$ organic mass concentrations (Chen et al., 2021) and are considered precursors for brown carbon formation (De Haan et al., 2017; Powelson et al., 2014). Three light mass-weighted amines, namely methylamine (MA), dimethylamine (DMA), and trimethylamine (TMA), are the most ubiquitous amines with annual emission of 96.2, 38.3, and 196.0 Gg, respectively (Yu and Luo, 2014). Nucleation of these amines with sulfuric acids is verified to play a profound role new particle formation in urban regions (Yao et al., 2018; Yin et al., 2021; Lian et al., 2020). Derived sulfate aerosols exhibit a cooling radiative forced effect (RFE) due to their strong light extinction, significantly affecting urban regional climates (Zhu et al., 2019).

Mineral particles are a dominant component of atmospheric aerosols with the annual emission of 1600 Tg (Andreae and Rosenfeld, 2008). Like sulfate aerosols, mineral particles also show strong light extinction and thus exhibit a cooling RFE on the atmosphere on a global scale. Moreover, anthropogenic organic pollutants (AOPs) including atmospheric amines are easily combined with mineral surface after uptake by mineral particles, which is confirmed by field measurements (Cheng et al., 2018), experimental observations (Huang et al., 2021), and theoretical calculations (Zhang et al., 2022). The formed AOP–mineral particle is found to exhibit a distinctive RFE from corresponding AOP aerosols and mineral particles (Yu et al., 2016). For example, the RFE of black carbon–mineral particle is $-112.9 \text{ W m}^{-2} \tau^{-1}$ in the lower-tropospheric layer, which is higher than that of individual black carbon ($-98.3 \text{ W m}^{-2} \tau^{-1}$) and mineral particles ($-101.0 \text{ W m}^{-2} \tau^{-1}$) (Tian et al., 2018b). The resulting net RFE of cooling on the lower atmosphere is enhanced by 7.4 % and 6.5 % compared to individual black carbon and mineral particles, respectively (Tian et al., 2018a).

AOP–mineral particles are easily oxidized through AOPs' heterogeneous oxidation reactions with atmospheric oxidants (Borduas et al., 2016; Nielsen et al., 2012; Onel et al., 2013, 2014). The oxidation state (OS) of AOPs thus grows higher because of oxygen addition into the parent AOPs or hydrogen removal from the initial AOPs (Kroll et al., 2015, 2011). Previous studies of individual AOP aerosols have confirmed that the light extinction–adsorption changes of oxidized aerosols–particles show strong correlations with the species and the OS of AOPs. For instance, one experimental study confirms that guaiacol-type aerosol's light adsorption is strengthened with the increased OS of guaiacol, but its light extinction is weakened, together leading to a stronger warming RFE of oxidized aerosol compared to that of initial aerosol (Lambe et al., 2013). Another experimental study states that the refractive indexes for α -pinene and *p*-xylene aerosols increase at low OS but decrease at high OS, finally resulting in 40 % RFE enhancement of oxidized aerosol based on that of initial aerosols (He et al., 2018). Like individual AOP aerosols, the increased OS of AOP could alter the light extinction and RFE of oxidized AOP–mineral particles, which have not been attempted.

In the present study, the correlations between amine's heterogeneous oxidation reaction and RFE of amine–mineral particle are comparably explored under clean and polluted conditions. MA, DMA, and TMA are employed as amine proxies considering their important contributions to secondary organic aerosol (SOA) formation. Kaolinite (Kao) is chosen as the proxy of mineral particle because of its large emission to the atmosphere (192.3 Tg yr^{-1}) (Tang et al., 2016). First, each amine uptake by the Kao particle is simulated using classical molecular dynamics (MD) methods. Subsequently, the thermodynamics and kinetics data of the heterogeneous oxidation reaction of each amine on the Kao surface are separately calculated under polluted and clean conditions using density functional theory (DFT). Accordingly, the OS of each amine is calculated under clean and polluted conditions. Next, the light extinction of amine–Kao particle at different OSs is characterized by refractive index (n) and extinction coefficient (p) at visible wavelengths (400–600 nm). Finally, the RFE changes of oxidized amine–Kao particles under different conditions are estimated and compared using the simple forcing efficiency (SFE) method (Bond and Bergstrom, 2007).

2 Models and methods

2.1 Classic MD simulations

Each amine uptake by Kao particle is simulated using the classical MD method. All the classical MD simulations are performed using the package of nanoscale MD (Phillips et al., 2005). Each amine–Kao system is equilibrated for 500 ps using NVT-MD methods, where CHARMM force fields are applied for MA, DMA, and TMA (Yang et al., 2017), re-

spectively, and a clay force field is used for Kao (Tenney and Cygan, 2014). NVT means number of atoms; volume and temperature are kept constant. The thermostat method of Langevin is used to control temperature at 298 K. A periodic boundary condition is applied to the system. A cutoff distance of 12.0 Å is used for Lennard-Jones and real-space Coulomb interactions. The particle-mesh Ewald method is also employed with the interpolation order of 6 with 1.0 Å grid spacing.

Based on the above MD trajectories, free-energy profiles of each amine–Kao particle are calculated using a weighted histogram analysis method (Kumar et al., 1995) based on umbrella sampling from the MD trajectory of each amine. The details are described in Sect. S1 in the Supplement.

2.2 DFT calculations

Static DFT calculations are carried out with the Vienna Ab initio Simulation Package (Kresse and Furthmüller, 1996a, b). Van der Waals interactions are described using the exchange–correlation functional of Perdew–Burke–Ernzerhof (PBE) generalized gradient approximation (GGA) (Perdew et al., 1992). The electron–core interactions are described with the projector augmented wave method. Simulated supercells are sampled with gamma-centered $3 \times 3 \times 1$ Monkhorst-Pack grids for the integration of the Brillouin zone. To ensure the efficiency and reliability of calculation, the kinetic cutoff energy is set at 400 eV, and the convergence criterion of structural optimization is $-0.01 \text{ eV } \text{Å}^{-1}$.

For DFT calculations, the initial electronic structures of amine–Kao particles are composed of the Kao surface and the amine molecule. The Kao surface is cleaved from the Kao unit cell along the (001) direction and expanded to the size of 2×1 . A vacuum zone of 15 Å is added onto the Kao surface to eliminate the interaction of each layer. MA, DMA, and TMA molecules are separately added above the Kao surface. Single point energies of amine–Kao ($\Delta E_{\text{amine–Kao}}$), amine (ΔE_{amine}), and the Kao surface (ΔE_{Kao}) are separately calculated. Therefore, the desorption energy of amine from the Kao surface (ΔE_{d}) equals $\Delta E_{\text{amine}} + \Delta E_{\text{Kao}} - \Delta E_{\text{amine–Kao}}$. The related results are listed in Fig. S2a–c in the Supplement.

For each amine–Kao system, the potential energy surface (PES) along each plausible oxidation path is calculated. Transition states (TSs) are confirmed with the climbing-image nudged elastic band method (Henkelman et al., 2000). The frequencies of reactants (RCs), TSs, and products and/or intermediates (Pros/IMs) are calculated, respectively. Thereby, RCs, Pros, and IMs are optimized structures with no imaginary frequency, and TSs are structures with one dominant imaginary frequency. Based on PES, energy barrier (ΔE^\ddagger) is $E_{\text{TS}} - E_{\text{RC}}$, and reaction energy (ΔE_{r}) is $E_{\text{Pro/IM}} - E_{\text{RC}}$. Based on ΔE^\ddagger and ΔE_{r} , k is described as

follows (Fernández-Ramos et al., 2007):

$$k = \sigma \kappa \frac{k_{\text{B}} T}{h} e^{-\frac{\Delta E^\ddagger}{RT}}, \quad (1)$$

$$k = \sigma \kappa \frac{k_{\text{B}} T}{h} \left(\frac{k_{\text{B}} T}{P_0} \right) e^{-\frac{\Delta E^\ddagger}{RT}}, \quad (2)$$

where Eq. (1) is for the first-order reaction constants, and Eq. (2) is for the second-order rate constants. σ is reaction path degeneracy, κ is the Eckart tunneling coefficient, k_{B} is the Boltzmann constant, T is the temperature, h is Planck's constant, and P_0 is standard atmospheric pressure. ΔE^\ddagger and k for each reaction step are displayed in Table S1 in the Supplement. The reaction steps, with ΔE^\ddagger lower than 20 kcal mol^{-1} and k higher than $1.38 \times 10^{-2} \text{ s}^{-1}$ (the first-order reaction) or $5.68 \times 10^{-22} \text{ s}^{-1} \text{ molec.}^{-1} \text{ cm}^3$ (the second-order reaction), are feasible under ambient conditions (Fernández-Ramos et al., 2007).

Based on DFT results, the n and p of each amine–Kao particle are calculated from a complex dielectric function (Fox and Bertsch, 2002) and a Kramers–Kronig relation (Gajdoš et al., 2006; Wang et al., 2021).

2.3 Oxidation state definition

Based on the proposed heterogeneous oxidation of atmospheric amine, the oxidation degree of amine is changed because of H removal and O addition. To quantify the oxidation degree, OS of amine is determined by $n_{\text{C–O}} - n_{\text{C–H}} - n_{\text{N–H}}$ (Kroll et al., 2015, 2011), where $n_{\text{C–O}}$, $n_{\text{C–H}}$, and $n_{\text{N–H}}$ indicate the number of C–O, C–H, and N–H bonds of amine and its oxidized products, respectively. Note that the OS of amine remains unchanged from $\text{RO}_2\cdot$ to $\text{RO}\cdot$ because no C–O, C–H, or N–H bond is formed or broken. To distinguish the same OSs, the suffixes of a and b are used. Likewise, the OS of amine remains unchanged from $\text{RO}_2\cdot$ to ROOOH . The suffixes c and d are used for distinction.

3 Results and discussion

3.1 Atmospheric amine uptake by Kao particles

Heterogeneous uptake of atmospheric amine by Kao particles under ambient conditions is simulated using the MD method, and the free-energy profile of each amine–Kao system is calculated based on the corresponding MD trajectories (Fig. S1a). Z represents the uptake distance between the mass center of the single amine molecule and the Kao surface. To each amine–Kao system, the free energy speeds up decreases when a specific amine gets close to the Kao surface, and it reaches 0 kcal mol^{-1} when the amine approaches the Kao surface ($Z = 3.0 \text{ Å}$), indicating that amine is more stable on the Kao surface than that in the gas phase. Such a decreased trend of free energy of the amine–Kao system explains that amine uptake by the Kao surface is feasible under

ambient conditions. Meanwhile, the corresponding ΔE_d values are 8.72, 6.41, and 6.85 kcal mol⁻¹ for MA–Kao, DMA–Kao, and TMA–Kao, respectively. Based on ΔE_d , rate constants are calculated by Eqs. (1) and (2). The adsorption rate constants of the three amines by Kao are 6.3×10^{-1} , 1.3×10^{-2} , and 2.7×10^{-2} cm³ molec.⁻¹ s⁻¹ based on adsorption energies of -8.72 , -6.41 , and -6.85 kcal mol⁻¹ (Fig. S5a–c). Field observations show that the concentration of Kao is 6.1×10^{21} cm⁻³ (Scanza et al., 2015). And the concentrations of amines are 2.5×10^8 , 2.7×10^7 , and 8.8×10^7 molec. cm⁻³ for MA, DMA, and TMA, respectively (Tan et al., 2018). Therefore, the adsorption rates of amines by Kao are in the range of 2.4×10^7 – 1.6×10^9 mol (L s)⁻¹, implying that these amines can be combined with the Kao surface under ambient conditions.

Along the uptake path, the relative concentration profile of each amine is calculated as $c(Z) = e^{-\Delta E/RT} c_{\text{gas}}$, where ΔE is read from the free-energy profile (Fig. S1a), c_{gas} is amine concentration in the gas phase, R represents ideal gas constant, and T is atmospheric temperature (298 K). The calculated relative concentration profile of each amine is shown in Fig. S1b. The results show that each amine concentration stays zero when Z is larger than 4.0 Å, and the concentration sharply increases when Z is smaller than 4.0 Å, indicating that amine uptake by the Kao surface readily occurs when amine is next to the Kao particle. The peaks of each amine concentration profile are located at approximately $Z = 3.0$ Å, and the related peak values for MA, DMA, and TMA on the Kao surface are, respectively, 1.0×10^4 , 1.0×10^4 , and 1.8×10^4 . These peak values are the final uptake concentration of amines by the Kao surface, which are 4 orders higher than the related amine concentration in the gas phase. This implies that heterogeneous oxidation of each amine on the mineral surface can compete with their gaseous oxidations, especially in the regions with abundant mineral particles (Uno et al., 2011).

To find out why each amine is more stable on the Kao surface than that in the gas phase, the interactions between amine and the Kao surface are analyzed using the charge density difference (CDD) method. As shown in Fig. S2a–c, the regions with increased electron density are shown in yellow, and the regions with decreased electron density are shown in blue. In each amine–Kao particle, the N atom of the relevant amine exhibits increased trends of electron density, and the regions around the H atom of the Kao surface present decreased trends of electron density. This means a strong combination exists between the N of each amine and the H of the Kao surface. Moreover, the measured distances between N and H are 1.81 Å in MA–Kao, 1.75 Å in DMA–Kao, and 1.75 Å in TMA–Kao particles (Fig. S2a–c), which are all shorter than 2.5 Å. By combining CCD and measured distance results, the hydrogen bond between N and H atoms in the amine–Kao particle is confirmed, contributing to stability of each amine on the Kao surface. This is also observed in other AOP–mineral particles (Zeitler et al., 2017; Roma-

nias et al., 2016). During the following oxidation reactions, the above hydrogen bonds keep amine or its derived products combined with the Kao particle, offering the possibility for amine to proceed heterogeneous oxidation on the Kao surface, affecting the extinction and RFE of amine–Kao particles.

3.2 Heterogeneous oxidation mechanism of atmospheric amines

On the Kao surface, the heterogeneous oxidation reactions of atmospheric amines are initiated by $\bullet\text{OH}$. $\bullet\text{OH}$ first binds with amines to form a pre-reactive complex, and the rate constants are 1.0×10^7 , 1.6×10^7 , and 1.7×10^8 cm³ molec.⁻¹ s⁻¹ based on reaction energies of -18.56 , -18.82 , and -20.23 kcal mol⁻¹ (Fig. 1a). The concentration of $\bullet\text{OH}$ is 2.4×10^6 molec. cm⁻³ in the atmosphere (Tan et al., 2018). Therefore, based on the kinetics calculation, the formation rate of the pre-reactive complex is in the range of 10.3–59.7 mol (L s)⁻¹. For MA and DMA, they each have two possible initial oxidation routes, i.e., H-abstraction routes from their methyl and amido groups. TMA only has the former H-abstraction route from the methyl group because its hydrogen in the amido group is completely substituted by the methyl group. The relevant PESs of two routes are compared in Fig. 1. All energy barriers and rate constants are summarized in Table S1. We first pay attention to MA's initial heterogeneous oxidation. Based on PES, the related k for the methyl route is calculated as 1.27×10^5 s⁻¹ molec.⁻¹ cm⁻³, which is 6 orders higher than that of the amido route (1.24×10^{-1} s⁻¹ molec.⁻¹ cm⁻³). Accordingly, the methyl route is dominant for MA's initial heterogeneous oxidation reaction. Agreements are observed in DMA's and TMA's heterogeneous oxidation reactions. However, for amines in the gas phase, the amido route is dominant (Onel et al., 2013). This is because the amido site is occupied by the H atom of the Kao surface (Fig. S2a–c). Accordingly, the Kao surface is found to alter the initial oxidation route of amines. Moreover, the present rate constants of heterogeneous initial oxidation reactions are much larger than those of the corresponding gaseous ones (Table S2). For instance, the related k for the heterogeneous initial oxidation reaction of DMA is calculated as 9.22 s⁻¹ molec.⁻¹ cm³, which is 11 orders higher than that of the gaseous one (Onel et al., 2013). Therefore, our results declare that the Kao surface significantly accelerates the initial oxidation reactions of atmospheric amines under ambient conditions.

Subsequently, the $\bullet\text{R}_C$ of each amine is separately converted into the corresponding amine–RO₂ \bullet through the O₂ addition, which is a barrierless reaction according to PESs (Fig. S3). Amine–RO₂ \bullet is further oxidized by different atmospheric oxidants under polluted and clean conditions. Under polluted conditions, each amine–RO₂ \bullet reacts with NO/O₂ following the steps of NO addition and H abstraction in order. Based on corresponding PESs (Fig. 2), the NO-addition

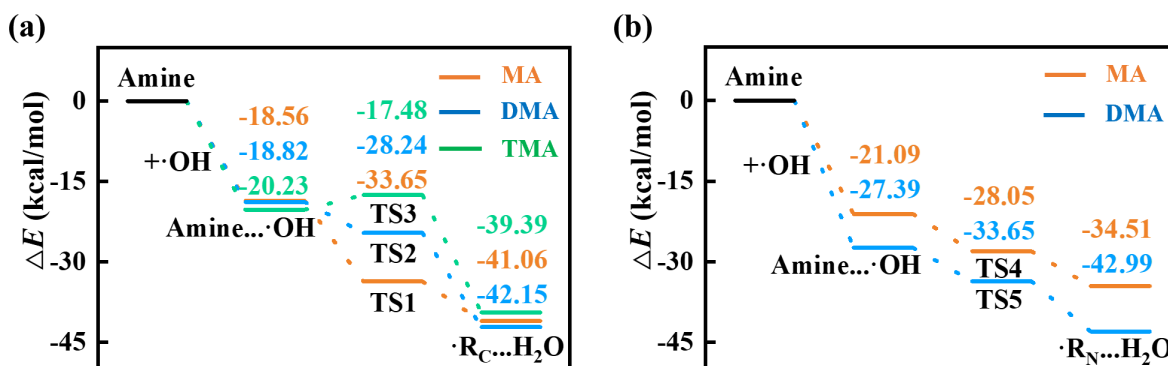


Figure 1. Initial oxidation reactions of amines with •OH. PESs of H-abstraction routes (a) from the methyl group and (b) from the amido group of MA, DMA, and TMA, respectively.

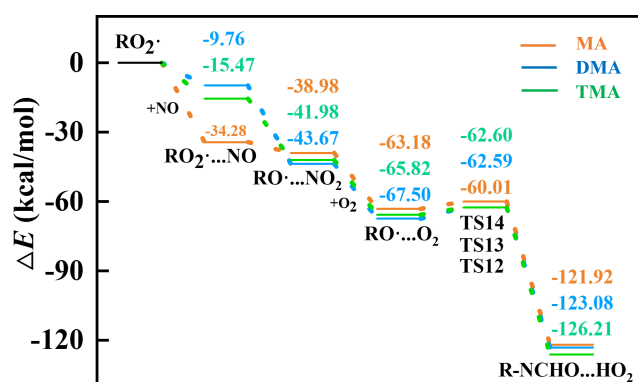


Figure 2. PESs of subsequent oxidation reactions of amine RO₂• with NO/O₂ under polluted conditions.

step is barrierless, and the energy barrier of H-abstraction step is positive, which are both feasible under ambient conditions. The low-oxygen-content product, i.e., RNCHO, is finally produced from each amine under polluted conditions. Compared to initial amines, the OS of each RNCHO increases by 4 under polluted conditions, as a result of the O addition to amine and H removal from amine.

Under clean conditions, MA-RO₂• or DMA-RO₂• could be further oxidized by O₂ through autoxidation or H-abstraction routes. First, the feasibility of MA-RO₂•'s oxidation by O₂ is investigated. Based on PES of the MA-RO₂•'s autoxidation route (orange line in Fig. 3a), the first H-transfer step is found to be the rate-limiting step with high ΔE^\ddagger of 27.38 kcal mol⁻¹, and the derived k_{17} is obtained as $1.34 \times 10^{-7} \text{ s}^{-1}$, indicating the autoxidation route is not feasible under ambient conditions. Similarly, the H-abstraction route of MA-RO₂• is also not feasible due to its high ΔE^\ddagger (Fig. S4). Like MA-RO₂•, the second H-transfer step of DMA-RO₂•'s autoxidation route (blue line in Fig. 3a) and H-abstraction route of DMA-RO₂• (Fig. S4) is not feasible due to its high ΔE^\ddagger . But the MA-RO₂• or DMA-RO₂• as an intermediate in the autoxidation route can be oxidized by

•OH to produce the high-oxygen-content product (Berndt et al., 2022), i.e., NH₂CH₂OOOH or HOOCH₂NHCH₂OOOH (Fig. 3b). This is a barrierless reaction, and ΔE_r is -27.16 or -32.06 kcal mol⁻¹, indicating the •OH addition of MA-RO₂• or DMA-RO₂• is feasible under ambient conditions. For MA and DMA, R-NCH₂OOOH with high oxygen content is the product under clean conditions. Compared to the initial MA and DMA, the OS of oxidized MA and DMA increases by 2 and 4 (Fig. 4).

Different from MA-RO₂• or DMA-RO₂•, TMA-RO₂• can only proceed autoxidation under clean conditions. This is because TMA's hydrogens are completely substituted by methyl groups, leading to no more H-abstraction sites on the nitrogen of TMA. TMA-RO₂•'s autoxidation is composed of H-transfer steps and O₂-addition steps. Based on PES (green line in Fig. 3a), the highest ΔE^\ddagger of the three H-transfer steps is obtained as 14.15 kcal mol⁻¹, and derived k is $2.23 \times 10^3 \text{ s}^{-1}$, indicating that the autoxidation is feasible under ambient conditions. The high-oxygen-content product, i.e., (HOOCH₂)₂NCHO, is finally produced from TMA under clean conditions. Compared to the initial TMA, the OS of oxidized TMA increases by 8 (Fig. 4), due to five O-atom additions to TMA from three O₂-addition steps.

Note that the NO concentration is important to determine amine heterogeneous oxidation mechanisms. As proposed under polluted conditions, amine-RO₂• and NO form a pre-reaction complex RO₂•...NO before the H-abstraction reaction (Fig. 2). The corresponding formation rate $r_{\text{RO}_2\cdot\cdot\cdot\text{NO}} = k_{\text{RO}_2\cdot\cdot\cdot\text{NO}}[\text{RO}_2\cdot][\text{NO}]$. Under clean conditions, the amine-RO₂• carries on the H transfer and forms •ROOH (Fig. 3a). The corresponding formation rate of •ROOH is $r_{\cdot\text{ROOH}} = k_{\cdot\text{ROOH}}[\text{RO}_2\cdot]$. $r_{\text{RO}_2\cdot\cdot\cdot\text{NO}}/r_{\cdot\text{ROOH}} > 10^3$ indicates that the H-abstraction reaction is dominant under polluted conditions, where the NO concentration should be higher than $k_{\cdot\text{ROOH}}/k_{\text{RO}_2\cdot\cdot\cdot\text{NO}} \times 10^3$. Conversely, $r_{\text{RO}_2\cdot\cdot\cdot\text{NO}}/r_{\cdot\text{ROOH}} < 10^{-3}$ implies that the autoxidation reaction is dominant under clean conditions, where the NO concentration is lower than $k_{\cdot\text{ROOH}}/k_{\text{RO}_2\cdot\cdot\cdot\text{NO}} \times 10^{-3}$. Specifically, for MA, $k_{\text{RO}_2\cdot\cdot\cdot\text{NO}} = 3.5 \times 10^6 \text{ cm}^3 \text{ molec.}^{-1} \text{ s}^{-1}$ and $k_{\cdot\text{ROOH}} = 5.2 \times$

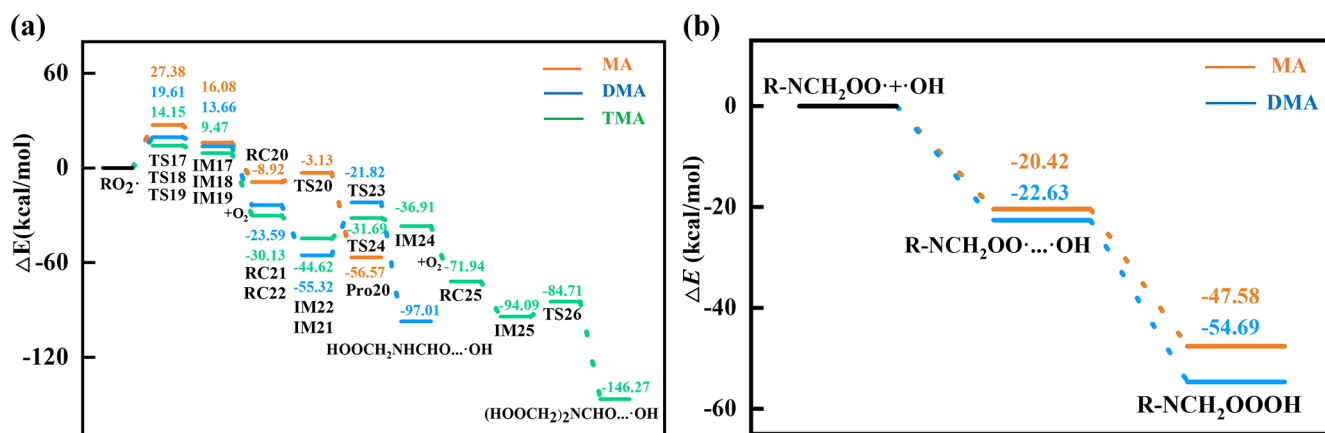


Figure 3. PESs of subsequent (a) autoxidation and (b) $\cdot\text{OH}$ addition of amine $\text{RO}_2\cdot$ under clean conditions.

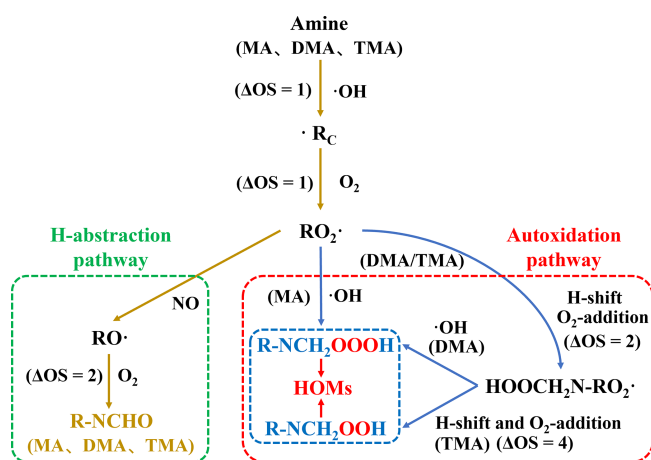


Figure 4. Proposed aging mechanism and related OS value changes for amine–Kao mixed particles under polluted (brown line) and clean (blue line) conditions.

10^{-3} s^{-1} ; for DMA, $k_{\text{RO}_2\cdot\cdot\text{NO}} = 3.7 \text{ cm}^3 \text{ molec.}^{-1} \text{ s}^{-1}$ and $k_{\cdot\text{ROOH}} = 2.6 \times 10^{-2} \text{ s}^{-1}$; and for TMA, $k_{\text{RO}_2\cdot\cdot\text{NO}} = 5.6 \times 10^4 \text{ cm}^3 \text{ molec.}^{-1} \text{ s}^{-1}$ and $k_{\cdot\text{ROOH}} = 2.6 \times 10^2 \text{ s}^{-1}$. Therefore, the NO concentration is determined to be higher than 1.5×10^{-6} , 7.2, and $4.7 \text{ molec. cm}^{-3}$ under polluted conditions and below 1.5×10^{-12} , 7.2×10^{-6} , and $4.7 \times 10^{-6} \text{ molec. cm}^{-3}$ under clean conditions, respectively. Therefore, for a mixture source of the three amines, all amines proceed H-abstraction reactions when the NO concentration is higher than $7.2 \text{ molec. cm}^{-3}$ and carry out an autoxidation reaction when the NO concentration is smaller than $1.5 \times 10^{-12} \text{ molec. cm}^{-3}$. Field observation shows that the concentration of NO in polluted conditions ranges from 4.1×10^6 – $1.9 \times 10^{13} \text{ molec. cm}^{-3}$. And when the concentration of NO is in the range of 5.2×10^{-9} – $7.8 \times 10^{-3} \text{ molec. cm}^{-3}$, it is considered relatively clean conditions (Tan et al., 2018). The corresponding field measure-

ment results are consistent with the theoretical calculation range.

In addition, the Kao particle is also found to reduce ΔE^\ddagger and increase k of the heterogeneous autoxidation of the TMA referred to gaseous autoxidation (Table S2). Specifically, the ΔE^\ddagger values of the three H-transfer steps during the heterogeneous autoxidation of the TMA are separately reduced by 1.85–3.65, 5.27–5.29, and 8.72–10.72 kcal mol^{-1} compared to different reported results, and the corresponding k values are obtained as 3, 4, and 8 orders higher than those in the gas phase (Ma et al., 2021; Moller et al., 2020), respectively. Therefore, compared to gaseous autoxidation of TMA, heterogeneous autoxidation is more feasible under ambient conditions, leading to abundant high OS products in oxidized amine–Kao particles. Moreover, during the whole heterogeneous oxidation under clean and polluted conditions, all oxidant intermediates and products stayed combined with the Kao surface (Fig. S5), leading to continuous influence on optical properties and RFE of amine–Kao particles.

3.3 Refractive index (n) and extinction coefficient (p)

Based on the proposed heterogeneous oxidation mechanisms (Fig. 4), the correlation of n/p of each oxidized amine–Kao particles and OS is separately calculated at visible wavelengths (400–600 nm). First, p changes of each amine–Kao particles are compared under clean and polluted conditions in Fig. 5. p of each amine–Kao particles stays equal to that of the Kao particle, implying that amine uptake has no effect on the Kao particle's light transmission. For example, at 400 nm, p is equal to 0.0012 for MA–Kao, DMA–Kao, and TMA–Kao (Fig. 5a–c), respectively, which is equal to that of the Kao particle. As amine oxidation starts, p of each oxidized amine–Kao particle slightly increases. For instance, at 400 nm, p of the oxidized TMA–Kao particle under polluted conditions increases to 0.002 at OS = –1 from 0.001 at OS = –9 (Fig. 5c), with a small $\Delta p = 0.001$ that can be ignored. One exception that p increases to 0.012 at OS = –8

exists, due to $\bullet R_C$ formation. However, $\bullet R_C$ is rapidly converted to molecule products, resulting in a temporary increase of p . p of oxidized MA–Kao and DMA–Kao also present similar changes under clean or polluted conditions (Fig. 5a and b). Accordingly, the heterogeneous uptake and oxidation of each amine have no influence on the amine–Kao particle's light transmission under ambient conditions.

Next, attention is paid to n changes of each amine–Kao particle. Like p changes with wavelengths, n of each oxidized amine–Kao particle decreases with the increased wavelength (Fig. S6a–c), which is similar to that of that observed for individual AOP aerosols (Flores et al., 2014; He et al., 2022; Jiang et al., 2019). However, different from p , the n of each amine–Kao particle is higher than that of the Kao particle (Fig. S6a–c), implying that amine uptake enhances Kao particle's light extinction.

Moreover, the n of TMA–Kao $>$ n of DMA–Kao $>$ n of MA–Kao may be determined by the molecular mass of amines. As heterogeneous oxidation proceeds, the n of each oxidized amine–Kao particle further increases with increased OS (Fig. 6) and shows distinctive profiles caused by different oxidation mechanisms. We first concentrate on n changes caused by H abstraction. The present results have declared that MA–Kao, DMA–Kao, and TMA–Kao particles under polluted conditions are oxidized through H-abstraction reactions. Figure 6a–c display that H abstraction induces very small n increments of these oxidized amine–Kao particles. For instance, for oxidized TMA–Kao particles, Δn at OS = -5 is 0.003 at 589 nm (Fig. 6c). Similar agreements are observed in oxidized MA–Kao and DMA–Kao particles. By contrast, autoxidation causes large n increments of oxidized amine–Kao particles. As shown in Fig. 6f, TMA–Kao's Δn at OS = -1 is 0.017 at 589 nm, which is at least 5 times larger under clean conditions than that of oxidized TMA–Kao particles under polluted conditions. Like TMA–Kao, MA–Kao and DMA–Kao particles also have a large Δn under clean conditions. The Δn of MA–Kao and DMA–Kao particles at OS = $-3d$ is 0.016 and 0.017 at 589 nm under clean conditions, which is 0.012 and 0.016 higher than under polluted conditions. Large Δn of oxidized amine–Kao particle is caused by a high-oxygen-content product with a high level of OS, resulting in strong extinction of amine–Kao particles under clean conditions.

3.4 Quantitative structure–property relationship analysis

To explain why n of oxidized amine–Kao particles increases more under clean conditions than that of any amine–Kao particles under polluted conditions, the molecular structure parameter changes with the increased OS under different conditions are compared using the quantitative structure–property relationship (QSPR) method reported from the reference (Redmond and Thompson, 2011). The molecular structure parameters include unsaturation (μ), polarizability (α), and molar mass (M) of all oxidation products with

different OSs, which are all positively associated with n of amine–Kao particles. Thereby, $\alpha = 1.51(\#C) + 0.17(\#H) + 0.57(\#O) + 1.05(\#N) + 0.32$, and $\mu = (\#C + 1) - 0.5(\#H - \#N)$, where #atom represents the number of specific atoms. The increments of these parameters are written as $\Delta\mu$, $\Delta\alpha$, and ΔM , respectively.

Figure 7a–c illustrate the structure parameter changes of MA, DMA, and TMA under polluted conditions. Specifically, as $\Delta OS = 4$, $\Delta\alpha$, ΔM , and $\Delta\mu$ of each amine are obtained as 0.23, 14, and 1 g mol^{-1} , respectively. These small increments of molecular mass, polarizability, and unsaturation account for slight enhancement of n of oxidized amine–Kao particles, which are derived from formations of RNCHO with low oxygen content under polluted conditions. Moreover, due to the same H-removal and O-addition levels of RNCHO based on related amine, these parameter increments are equal. This suggests that, under polluted conditions, n increments of oxidized amine–Kao particles are more determined by the oxidation process but are little related to amine structures.

More attention is paid to the structure parameter changes of amine under clean conditions. Compared to the initial TMA, $\Delta\alpha$ and ΔM are obtained as 2.51 and 78 g mol^{-1} separately (Fig. 7f), which are about 11 and 6 times larger those under polluted conditions. Similarly, MA's or DMA's $\Delta\alpha$ and ΔM under clean conditions are larger than under polluted conditions. Amine under clean conditions is confirmed to carry out autoxidation on the Kao surface in this work, producing high-oxygen-content products ($\text{NH}_2\text{CH}_2\text{OOH}$, $\text{HOOCH}_2\text{NHCH}_2\text{OOH}$, and $(\text{HOOCH}_2)_2\text{NCHO}$). Therefore, significant increments of molecule mass and polarizability together contribute a large n of oxidized amine–Kao particles, resulting in strong extinction under clean conditions. This is also observed in oxidized naphthalene aerosol (He et al., 2022).

3.5 Enhanced simple forcing efficiency

Based on obtained n increments (Fig. 6), SFE (Bond and Bergstrom, 2007) is calculated to quantify the influence of heterogeneous uptake and oxidations of each amine on Kao particles under clean and polluted conditions. ΔSFE is defined as the ratio of SFE of oxidized amine–Kao particles to that of individual Kao particles. Note that, at the same wavelength and OS, p is at least 3 orders smaller than n of the same amine–Kao particle. For example, for the TMA–Kao particle at 600 nm, the p is less than 0.001 at any OS of TMA (Fig. 5c), and the corresponding n stays larger than 1.25 (Fig. 6c and f). Therefore, p is ignored when evaluating SFE of amine–Kao particles. The related derivations of SFE and ΔSFE are given in Sect. S2 in the Supplement.

Amine uptake enhances the cooling RFE of amine–Kao particles at 400–600 nm, which is proven by high levels of ΔSFE profiles for each amine–Kao particle (black curves in Fig. S7). Specifically, ΔSFE is obtained as 12.0% for

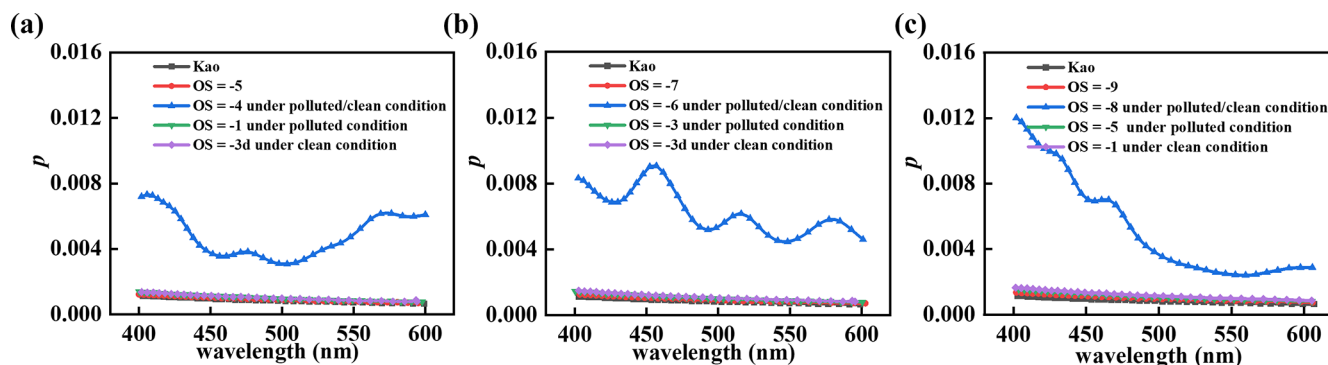


Figure 5. p changes of each amine–Kao particle with increased wavelength (400–600 nm) under polluted and clean conditions. Results for (a) MA–Kao, (b) DMA–Kao, and (c) TMA–Kao particles, respectively.

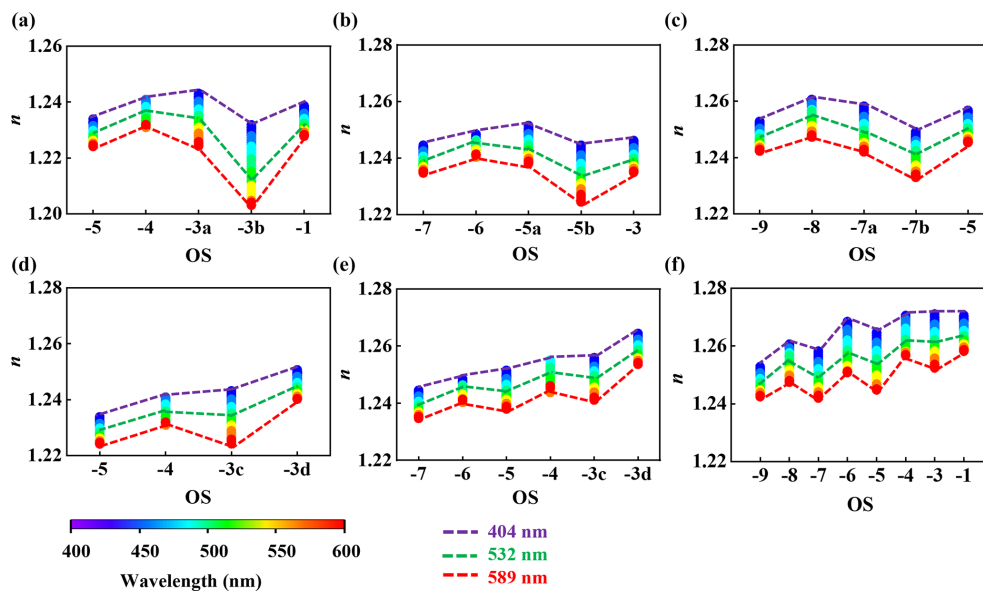


Figure 6. The relationship between n and OS in the wavelength range of 400–600 nm under polluted (a–c) and clean (d–f) conditions. Related profiles are for (a, d) MA–Kao (b, e) DMA–Kao, and (c, f) TMA–Kao mixed particles, respectively. Three trend lines in colors of purple, green, and red mark wavelengths of 404, 532, and 589 nm, respectively.

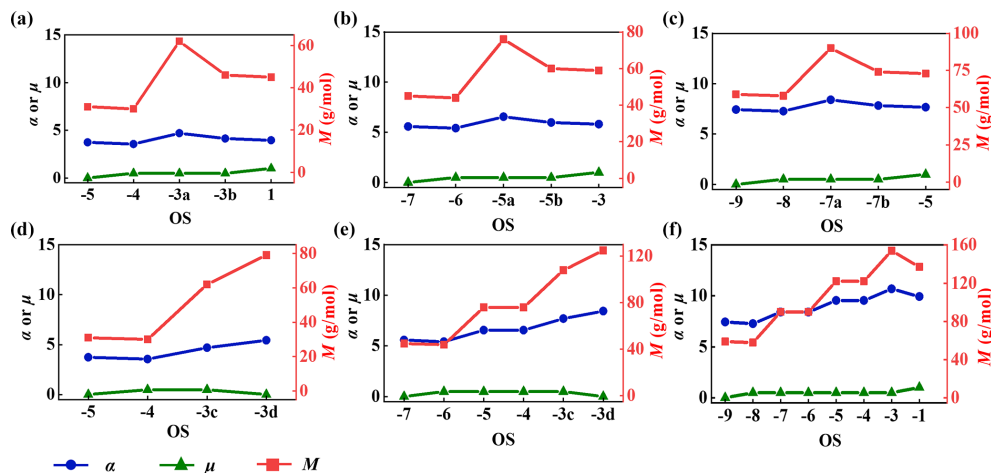


Figure 7. The molecular structure parameter changes with the increased OS during (a–c) H abstraction and (d–f) autoxidation.

MA–Kao particles, 22.0 % for DMA–Kao particles, and 29.5 % for TMA–Kao particles, respectively. Δ SFE is furthermore increased after amine oxidation under polluted and clean conditions. For example, at 400–600 nm, Δ SFE of oxidized TMA–Kao particles is obtained as 32.0 %–33.6 % under polluted conditions (red curve in Fig. S7c) and 45.6 %–47.1 % under clean conditions (blue curve in Fig. S7c). The same increase also occurs in MA–Kao or DMA–Kao oxidation. Δ SFE of oxidized MA–Kao or DMA–Kao particles is obtained as 15.4 %–16.2 % or 22.1 %–23.1 % under polluted conditions (red curve in Fig. S7a and b) and 27.1 %–27.5 % or 40.9 %–41.4 % under clean conditions (blue curve in Fig. S7a and b). Compared to that under polluted conditions, the larger Δ SFE of oxidized amine–Kao particles under clean conditions is attributed to stronger particle extinction, due to high-oxygen-content product formation.

4 Conclusions

In summary, heterogeneous uptake and oxidation of amines on the Kao surface are completely investigated under clean and polluted conditions using DFT methods, and their enhanced effects on cooling RFE of amine–Kao particles on the atmosphere are first confirmed. Like other AOPs (Borduas et al., 2016; Nielsen et al., 2012; Onel et al., 2013, 2014), amine uptake by Kao particles is feasible, and heterogeneous oxidation reactions are found to be more competitive than gaseous oxidation reactions, leading to an increase in oxygen content of amine–Kao particles in the atmosphere. After amine uptake, compared to Kao particles, SFE is enhanced by 12 %–29.5 % for amine–Kao particles, suggesting amine uptake enhances cooling RFE of Kao particles on the atmosphere. Amine's heterogeneous oxidation reactions are found to furthermore enhance Kao's cooling RFE, due to the increase in oxygen content of amine–Kao particles. More importantly, under clean conditions with low NO concentrations, the SFE of oxidized amine–Kao particle is enhanced by 27.1 %–47.1 %, which is at least 11.3 %–18.8 % higher than that of amine–Kao particles under polluted conditions. The significant cooling RFE enhancement of oxidized amine–Kao particles is the result of a high-oxygen-content product generated from amine autoxidation. This conclusion can be deduced to other AOPs with complete hydrogen substitution by methyl groups, such as triethylamine (Ma et al., 2021), dimethyl sulfide (Berndt et al., 2019; Wu et al., 2015; Veres et al., 2020), and dimethyl ether (Wang and Wang, 2016), which prefer to experience autoxidation under clean conditions.

Amines are commonly confirmed as precursors for brown carbon formation (De Haan et al., 2017; Powelson et al., 2014), and lots of attention is paid to their contributions to light-adsorbing and warming RFE on the atmosphere. However, our results propose amines can enhance cooling RFE on the atmosphere, especially under clean conditions, through

heterogeneous uptake and oxidation reactions on mineral particles. Considering large amounts of mineral particles in the atmosphere (Andreae and Rosenfeld, 2008) and their inherent cooling RFE on global scale, the proposed cooling RFE derived from atmospheric amines can be equally important to their warming RFE on the atmosphere. Therefore, it is necessary to update heterogeneous oxidation mechanism and kinetics data of amines in order to accurately evaluate related comprehensive RFE on the atmosphere.

Code availability. The software code is not publicly accessible. The package of nanoscale MD is required to simulate the heterogeneous uptake of atmospheric amine by Kao particles. The Vienna Ab initio Simulation Package is required to carry out DFT calculations.

Data availability. The calculated data in this work are provided in Table S1.

Supplement. The supplement related to this article is available online at: <https://doi.org/10.5194/acp-24-9019-2024-supplement>.

Author contributions. WZ and TA designed the research goals, aims, and methodology. JM and ZF contributed to calculations and data processing. WZ analyzed the data and wrote the manuscript. WZ, JM, ZF, YoJ, YuJ, YG, GL, and TA proofread and commented on the paper.

Competing interests. The contact author has declared that none of the authors has any competing interests.

Disclaimer. Publisher's note: Copernicus Publications remains neutral with regard to jurisdictional claims made in the text, published maps, institutional affiliations, or any other geographical representation in this paper. While Copernicus Publications makes every effort to include appropriate place names, the final responsibility lies with the authors.

Financial support. This research has been supported by the National Natural Science Foundation of China (NSFC), Major International Joint Research Programme (grant nos. 42020104001, 42277081, and 42077189), the Basic and Applied Basic Research Fund Project of Guangdong Province (grant nos. 2024A1515012691 and 2019B151502064), the National Key Research and Development Program of China (grant no. 2022YFC3105600), and the Guangdong Provincial Key R&D Program (grant no. 2022-GDUT-A0007).

Review statement. This paper was edited by Guangjie Zheng and reviewed by two anonymous referees.

References

- Andreae, M. O. and Rosenfeld, D.: Aerosol–cloud–precipitation interactions. Part I. The nature and sources of cloud-active aerosols, *Earth-Sci. Rev.*, 89, 13–41, <https://doi.org/10.1016/j.earscirev.2008.03.001>, 2008.
- Berndt, T., Scholz, W., Mentler, B., Fischer, L., Hoffmann, E. H., Tilgner, A., Hyttinen, N., Prisle, N. L., Hansel, A., and Herrmann, H.: Fast Peroxy Radical Isomerization and OH Recycling in the Reaction of OH Radicals with Dimethyl Sulfide, *Physical Chemistry Letters*, 10, 6478–6483, <https://doi.org/10.1021/acs.jpcclett.9b02567>, 2019.
- Berndt, T., Chen, J., Kjaergaard, E. R., Moller, K. H., Tilgner, A., Hoffmann, E. H., Herrmann, H., Crouse, J. D., Wennberg, P. O., and Kjaergaard, H. G.: Hydrotrioxide (ROOOH) formation in the atmosphere, *Science*, 376, 979–982, <https://doi.org/10.1126/science.abn6012>, 2022.
- Bond, T. C. and Bergstrom, R. W.: Light Absorption by Carbonaceous Particles: An Investigative Review, *Aerosol Sci. Tech.*, 40, 27–67, <https://doi.org/10.1080/02786820500421521>, 2007.
- Borduas, N., Abbatt, J. P., Murphy, J. G., So, S., and da Silva, G.: Gas-Phase Mechanisms of the Reactions of Reduced Organic Nitrogen Compounds with OH Radicals, *Environ. Sci. Technol.*, 50, 11723–11734, <https://doi.org/10.1021/acs.est.6b03797>, 2016.
- Chen, W., Ye, Y. Q., Hu, W. W., Zhou, H. S., Pan, T. L., Wang, Y. K., Song, W., Song, Q. C., Ye, C. S., Wang, C. M., Wang, B. L., Huang, S., Yuan, B., Zhu, M., Lian, X. F., Zhang, G. H., Bi, X. H., Jiang, F., Liu, J. W., Canonaco, F., Prevot, A. S. H., Shao, M., and Wang, X. M.: Real-Time Characterization of Aerosol Compositions, Sources, and Aging Processes in Guangzhou During PRIDE-GBA 2018 Campaign, *J. Geophys. Res.-Atmos.*, 126, e2021JD035114, <https://doi.org/10.1029/2021JD035114>, 2021.
- Cheng, C., Huang, Z., Chan, C. K., Chu, Y., Li, M., Zhang, T., Ou, Y., Chen, D., Cheng, P., Li, L., Gao, W., Huang, Z., Huang, B., Fu, Z., and Zhou, Z.: Characteristics and mixing state of amine-containing particles at a rural site in the Pearl River Delta, China, *Atmos. Chem. Phys.*, 18, 9147–9159, <https://doi.org/10.5194/acp-18-9147-2018>, 2018.
- De Haan, D. O., Hawkins, L. N., Welsh, H. G., Pednekar, R., Casar, J. R., Pennington, E. A., de Loera, A., Jimenez, N. G., Symons, M. A., Zauscher, M., Pajunoja, A., Caponi, L., Cazau-nau, M., Formenti, P., Gratien, A., Pangui, E., and Doussin, J. F.: Brown Carbon Production in Ammonium- or Amine-Containing Aerosol Particles by Reactive Uptake of Methylglyoxal and Photolytic Cloud Cycling, *Environ. Sci. Technol.*, 51, 7458–7466, <https://doi.org/10.1021/acs.est.7b00159>, 2017.
- Fernández-Ramos, A., Ellington, B. A., Meana-Pañeda, R., Marques, J. M. C., and Truhlar, D. G.: Symmetry numbers and chemical reaction rates, *Theor. Chem. Acc.*, 118, 813–826, <https://doi.org/10.1007/s00214-007-0328-0>, 2007.
- Flores, J. M., Zhao, D. F., Segev, L., Schlag, P., Kiendler-Scharr, A., Fuchs, H., Watne, Å. K., Bluvshstein, N., Mentel, Th. F., Hallquist, M., and Rudich, Y.: Evolution of the complex refractive index in the UV spectral region in ageing secondary organic aerosol, *Atmos. Chem. Phys.*, 14, 5793–5806, <https://doi.org/10.5194/acp-14-5793-2014>, 2014.
- Fox, M. and Bertsch, G. F.: Optical Properties of Solids, *Am. J. Phys.*, 70, 1269–1270, <https://doi.org/10.1119/1.1691372>, 2002.
- Gajdoš, M., Hummer, K., Kresse, G., Furthmüller, J., and Bechstedt, F.: Linear optical properties in the projector-augmented wave methodology, *Phys. Rev. B*, 73, 45112–45121, <https://doi.org/10.1103/PhysRevB.73.045112>, 2006.
- He, Q., Bluvshstein, N., Segev, L., Meidan, D., Flores, J. M., Brown, S. S., Brune, W., and Rudich, Y.: Evolution of the Complex Refractive Index of Secondary Organic Aerosols during Atmospheric Aging, *Environ. Sci. Technol.*, 52, 3456–3465, <https://doi.org/10.1021/acs.est.7b05742>, 2018.
- He, Q., Li, C., Siemens, K., Morales, A. C., Hettiyadura, A. P. S., Laskin, A., and Rudich, Y.: Optical Properties of Secondary Organic Aerosol Produced by Photooxidation of Naphthalene under NO_x Condition, *Environ. Sci. Technol.*, 56, 4816–4827, 2022.
- Henkelman, G., Uberuaga, B. P., and Jónsson, H.: A climbing image nudged elastic band method for finding saddle points and minimum energy paths, *J. Chem. Phys.*, 113, 9901–9904, <https://doi.org/10.1063/1.1329672>, 2000.
- Huang, Y. Z., Mahrt, F., Xu, S., Shiraiwa, M., Zuend, A., and Bertram, A. K.: Coexistence of three liquid phases in individual atmospheric aerosol particles, *P. Natl. Acad. Sci. USA*, 118, 9, <https://doi.org/10.1073/pnas.2102512118>, 2021.
- Jiang, H., Frie, A. L., Lavi, A., Chen, J. Y., Zhang, H., Bahreini, R., and Lin, Y.-H.: Brown Carbon Formation from Nighttime Chemistry of Unsaturated Heterocyclic Volatile Organic Compounds, *Environ. Sci. Tech. Lett.*, 6, 184–190, <https://doi.org/10.1021/acs.estlett.9b00017>, 2019.
- Kresse, G. and Furthmüller, J.: Efficiency of ab-initio total energy calculations for metals and semiconductors using a plane-wave basis set, *Comp. Mater. Sci.*, 6, 15–50, 1996a.
- Kresse, G. and Furthmüller, J.: Efficient iterative schemes for ab initio total-energy calculations using a plane-wave basis set, *Phys. Rev. B*, 54, 11169–11186, 1996b.
- Kroll, J. H., Donahue, N. M., Jimenez, J. L., Kessler, S. H., Canagaratna, M. R., Wilson, K. R., Altieri, K. E., Mazzoleni, L. R., Wozniak, A. S., Bluhm, H., Mysak, E. R., Smith, J. D., Kolb, C. E., and Worsnop, D. R.: Carbon oxidation state as a metric for describing the chemistry of atmospheric organic aerosol, *Nat. Chem.*, 3, 133–139, <https://doi.org/10.1038/nchem.948>, 2011.
- Kroll, J. H., Lim, C. Y., Kessler, S. H., and Wilson, K. R.: Heterogeneous Oxidation of Atmospheric Organic Aerosol: Kinetics of Changes to the Amount and Oxidation State of Particle-Phase Organic Carbon, *J. Phys. Chem. A*, 119, 10767–10783, <https://doi.org/10.1021/acs.jpca.5b06946>, 2015.
- Kumar, S., Rosenberg, J. M., Bouzida, D., Swendsen, R. H., and Kollman, P.: Multidimensional free-energy calculations using the weighted histogram analysis method, *J. Comput. Chem.*, 16, 1339–1350, 1995.
- Lambe, A. T., Cappa, C. D., Massoli, P., Onasch, T. B., Forestieri, S. D., Martin, A. T., Cummings, M. J., Croasdale, D. R., Brune, W. H., Worsnop, D. R., and Davidovits, P.: Relationship between Oxidation Level and Optical Properties of Secondary Organic Aerosol, *Environ. Sci. Technol.*, 47, 6349–6357, <https://doi.org/10.1021/es401043j>, 2013.
- Lian, X., Zhang, G., Lin, Q., Liu, F., Peng, L., Yang, Y., Fu, Y., Jiang, F., Bi, X., Chen, D., Wang, X., Peng, P. A., and Sheng, G.: Seasonal variation of amine-containing particles

- in urban Guangzhou, China, *Atmos. Environ.*, 222, 117102, <https://doi.org/10.1016/j.atmosenv.2019.117102>, 2020.
- Ma, F. F., Xie, H. B., Li, M. X., Wang, S. N., Zhang, R. Y., and Chen, J. W.: Autoxidation mechanism for atmospheric oxidation of tertiary amines: Implications for secondary organic aerosol formation, *Chemosphere*, 273, 129207, <https://doi.org/10.1016/j.chemosphere.2020.129207>, 2021.
- Moller, K. H., Berndt, T., and Kjaergaard, H. G.: Atmospheric Autoxidation of Amines, *Environ. Sci. Technol.*, 54, 11087–11099, <https://doi.org/10.1021/acs.est.0c03937>, 2020.
- Nielsen, C. J., Herrmann, H., and Weller, C.: Atmospheric chemistry and environmental impact of the use of amines in carbon capture and storage (CCS), *Chem. Soc. Rev.*, 41, 6684–6704, <https://doi.org/10.1039/c2cs35059a>, 2012.
- Onel, L., Thonger, L., Blitz, M. A., Seakins, P. W., Bunkan, A. J., Solimannejad, M., and Nielsen, C. J.: Gas-phase reactions of OH with methyl amines in the presence or absence of molecular oxygen. An experimental and theoretical study, *J. Phys. Chem. A*, 117, 10736–10745, <https://doi.org/10.1021/jp406522z>, 2013.
- Onel, L., Blitz, M., Dryden, M., Thonger, L., and Seakins, P.: Branching ratios in reactions of OH radicals with methylamine, dimethylamine, and ethylamine, *Environ. Sci. Technol.*, 48, 9935–9942, <https://doi.org/10.1021/es502398r>, 2014.
- Perdew, J. P., Chevary, J. A., Vosko, S. H., Jackson, K. A., Pederson, M. R., Singh, D. J., and Fiolhais, C.: Atoms, molecules, solids, and surfaces: Applications of the generalized gradient approximation for exchange and correlation, *Phys. Rev. B*, 46, 6671–6687, <https://doi.org/10.1103/physrevb.46.6671>, 1992.
- Phillips, J. C., Braun, R., Wang, W., Gumbart, J., Tajkhorshid, E., Villa, E., Chipot, C., Skeel, R. D., Kale, L., and Schulten, K.: Scalable molecular dynamics with NAMD, *J. Comput. Chem.*, 26, 1781–1802, <https://doi.org/10.1002/jcc.20289>, 2005.
- Powelson, M. H., Espelien, B. M., Hawkins, L. N., Galloway, M. M., and De Haan, D. O.: Brown Carbon Formation by Aqueous-Phase Carbonyl Compound Reactions with Amines and Ammonium Sulfate, *Environ. Sci. Technol.*, 48, 985–993, <https://doi.org/10.1021/es4038325>, 2014.
- Redmond, H. and Thompson, J. E.: Evaluation of a quantitative structure-property relationship (QSPR) for predicting mid-visible refractive index of secondary organic aerosol (SOA), *Phys. Chem. Chem. Phys.*, 13, 6872–6882, <https://doi.org/10.1039/c0cp02270e>, 2011.
- Romanias, M. N., Ourrad, H., Thevenet, F., and Riffault, V.: Investigating the Heterogeneous Interaction of VOCs with Natural Atmospheric Particles: Adsorption of Limonene and Toluene on Saharan Mineral Dusts, *J. Phys. Chem. A*, 120, 1197–1212, <https://doi.org/10.1021/acs.jpca.5b10323>, 2016.
- Scanza, R. A., Mahowald, N., Ghan, S., Zender, C. S., Kok, J. F., Liu, X., Zhang, Y., and Albani, S.: Modeling dust as component minerals in the Community Atmosphere Model: development of framework and impact on radiative forcing, *Atmos. Chem. Phys.*, 15, 537–561, <https://doi.org/10.5194/acp-15-537-2015>, 2015.
- Tan, Z., Rohrer, F., Lu, K., Ma, X., Bohm, B., Broch, S., Dong, H., Fuchs, H., Gkatzelis, G. I., Hofzumahaus, A., Holland, F., Li, X., Liu, Y., Liu, Y., Novelli, A., Shao, M., Wang, H., Wu, Y., Zeng, L., Hu, M., Kiendler-Scharr, A., Wahner, A., and Zhang, Y.: Wintertime photochemistry in Beijing: observations of RO_x radical concentrations in the North China Plain during the BEST-ONE campaign, *Atmos. Chem. Phys.*, 18, 12391–12411, <https://doi.org/10.5194/acp-18-12391-2018>, 2018.
- Tang, M., Cziczco, D. J., and Grassian, V. H.: Interactions of Water with Mineral Dust Aerosol: Water Adsorption, Hygroscopicity, Cloud Condensation, and Ice Nucleation, *Chem. Rev.*, 116, 4205–4259, <https://doi.org/10.1021/acs.chemrev.5b00529>, 2016.
- Tenney, C. M. and Cygan, R. T.: Molecular Simulation of Carbon Dioxide, Brine, and Clay Mineral Interactions and Determination of Contact Angles, *Environ. Sci. Technol.*, 48, 2035–2042, <https://doi.org/10.1021/es404075k>, 2014.
- Tian, P., Zhang, L., Cao, X. J., Sun, N. X., Mo, X. Y., Liang, J. N., Li, X. T., Gao, X. G., Zhang, B. D., and Wang, H.: Enhanced Bottom-of-the-Atmosphere Cooling and Atmosphere Heating Efficiency by Mixed-Type Aerosols: A Classification Based on Aerosol Nonsphericity, *J. Atmos. Sci.*, 75, 113–124, <https://doi.org/10.1175/Jas-D-17-0019.1>, 2018a.
- Tian, P., Zhang, L., Ma, J., Tang, K., Xu, L., Wang, Y., Cao, X., Liang, J., Ji, Y., Jiang, J. H., Yung, Y. L., and Zhang, R.: Radiative absorption enhancement of dust mixed with anthropogenic pollution over East Asia, *Atmos. Chem. Phys.*, 18, 7815–7825, <https://doi.org/10.5194/acp-18-7815-2018>, 2018b.
- Uno, I., Eguchi, K., Yumimoto, K., Liu, Z., Hara, Y., Sugimoto, N., Shimizu, A., and Takemura, T.: Large Asian dust layers continuously reached North America in April 2010, *Atmos. Chem. Phys.*, 11, 7333–7341, <https://doi.org/10.5194/acp-11-7333-2011>, 2011.
- Veres, P. R., Neuman, J. A., Bertram, T. H., Assaf, E., Wolfe, G. M., Williamson, C. J., Weinzierl, B., Tilmes, S., Thompson, C. R., Thames, A. B., Schroder, J. C., Saiz-Lopez, A., Rollins, A. W., Roberts, J. M., Price, D., Peischl, J., Nault, B. A., Moller, K. H., Miller, D. O., Meinardi, S., Li, Q., Lamarque, J. F., Kupc, A., Kjaergaard, H. G., Kinnison, D., Jimenez, J. L., Jernigan, C. M., Hornbrook, R. S., Hills, A., Dollner, M., Day, D. A., Cuevas, C. A., Campuzano-Jost, P., Burkholder, J., Bui, T. P., Brune, W. H., Brown, S. S., Brock, C. A., Bourgeois, I., Blake, D. R., Apel, E. C., and Ryerson, T. B.: Global airborne sampling reveals a previously unobserved dimethyl sulfide oxidation mechanism in the marine atmosphere, *P. Natl. Acad. Sci. USA*, 117, 4505–4510, <https://doi.org/10.1073/pnas.1919344117>, 2020.
- Wang, S. and Wang, L.: The atmospheric oxidation of dimethyl, diethyl, and diisopropyl ethers. The role of the intramolecular hydrogen shift in peroxy radicals, *Phys. Chem. Chem. Phys.*, 18, 7707–7714, <https://doi.org/10.1039/c5cp07199b>, 2016.
- Wang, V., Xu, N., Liu, J.-C., Tang, G., and Geng, W.-T.: VASPKIT: A user-friendly interface facilitating high-throughput computing and analysis using VASP code, *Comput. Phys. Commun.*, 267, 267–286, <https://doi.org/10.1016/j.cpc.2021.108033>, 2021.
- Wu, R., Wang, S., and Wang, L.: New mechanism for the atmospheric oxidation of dimethyl sulfide. The importance of intramolecular hydrogen shift in a CH₃SCH₂OO radical, *J. Phys. Chem. A*, 119, 112–117, <https://doi.org/10.1021/jp511616j>, 2015.
- Yang, X., Rees, R. J., Conway, W., Puxty, G., Yang, Q., and Winkler, D. A.: Computational Modeling and Simulation of CO₂ Capture by Aqueous Amines, *Chem. Rev.*, 117, 9524–9593, <https://doi.org/10.1021/acs.chemrev.6b00662>, 2017.
- Yao, L., Garmash, O., Bianchi, F., Zheng, J., Yan, C., Kontkanen, J., Junninen, H., Mazon, S. B., Ehn, M., Paasonen, P., Sipila, M., Wang, M., Wang, X., Xiao, S., Chen, H., Lu, Y., Zhang, B.,

- Wang, D., Fu, Q., Geng, F., Li, L., Wang, H., Qiao, L., Yang, X., Chen, J., Kerminen, V. M., Petaja, T., Worsnop, D. R., Kulmala, M., and Wang, L.: Atmospheric new particle formation from sulfuric acid and amines in a Chinese megacity, *Science*, 361, 278–281, <https://doi.org/10.1126/science.aao4839>, 2018.
- Yin, R., Yan, C., Cai, R., Li, X., Shen, J., Lu, Y., Schobesberger, S., Fu, Y., Deng, C., Wang, L., Liu, Y., Zheng, J., Xie, H., Bianchi, F., Worsnop, D. R., Kulmala, M., and Jiang, J.: Acid-Base Clusters during Atmospheric New Particle Formation in Urban Beijing, *Environ. Sci. Technol.*, 55, 10994–11005, <https://doi.org/10.1021/acs.est.1c02701>, 2021.
- Yu, F. and Luo, G.: Modeling of gaseous methylamines in the global atmosphere: impacts of oxidation and aerosol uptake, *Atmos. Chem. Phys.*, 14, 12455–12464, <https://doi.org/10.5194/acp-14-12455-2014>, 2014.
- Yu, X., Lu, R., Kumar, K. R., Ma, J., Zhang, Q., Jiang, Y., Kang, N., Yang, S., Wang, J., and Li, M.: Dust aerosol properties and radiative forcing observed in spring during 2001–2014 over urban Beijing, China, *Environ. Sci. Pollut. R.*, 23, 15432–15442, <https://doi.org/10.1007/s11356-016-6727-9>, 2016.
- Zeitler, T. R., Greathouse, J. A., Cygan, R. T., Fredrich, J. T., and Jerauld, G. R.: Molecular Dynamics Simulation of Resin Adsorption at Kaolinite Edge Sites: Effect of Surface Deprotonation on Interfacial Structure, *J. Phys. Chem. C*, 121, 22787–22796, <https://doi.org/10.1021/acs.jpcc.7b06688>, 2017.
- Zhang, W., Guo, Z., Zhang, W., Ji, Y., Li, G., and An, T.: Contribution of reaction of atmospheric amine with sulfuric acid to mixing particle formation from clay mineral, *Sci. Total Environ.*, 821, 821–830, <https://doi.org/10.1016/j.scitotenv.2022.153336>, 2022.
- Zhu, J., Penner, J. E., Yu, F., Sillman, S., Andreae, M. O., and Coe, H.: Decrease in radiative forcing by organic aerosol nucleation, climate, and land use change, *Nat. Commun.*, 10, 423, <https://doi.org/10.1038/s41467-019-08407-7>, 2019.